



Field: Mechanical Engineering

PhD THESIS

- ABSTRACT -

Optimisation of Currents Through Expanding Corners in Wind and Water Tunnels

PhD Student:
Alexander François Urban
Baron Vielhauer von Hohenhau

PhD Supervisor:
Prof. Eng. Vasile Năsui, PhD

Examination committee:

Chair:

Prof. Eng. **Mircea Cristian Dudescu**, PhD – Technical University of Cluj-Napoca;

PhD Supervisor:

Prof. Eng. **Vasile Năsui**, PhD – Technical University of Cluj-Napoca;

Members:

Prof. Eng. **Sanda-Carmen Georgescu**, PhD – National University of Science and Technology
POLITEHNICA Bucharest;

Prof. Eng. **Ilare Bordeasu**, PhD – Polytechnic University of Timișoara;

Prof. Eng. **Dan Opruța**, PhD – Technical University of Cluj-Napoca.

- Cluj-Napoca -
2023

TABLE OF CONTENTS

Summary of the Doctoral Thesis	2
1. Introduction.....	2
1.1. Motivation	2
1.2. Objectives and Purpose	2
1.3. Scientific Novelty.....	3
2. Current State of Knowledge.....	3
2.1. Diffusers.....	3
2.2. Expansion Vanes	5
3. Theoretical Contributions.....	5
3.1. Developing the Theoretical Vane Shape	6
3.2. Conducting CFD Simulations.....	7
4. Practical Contributions	8
4.1. Constructing the vanes	8
4.2. Constructing a Wind Tunnel	11
4.3. Constructing the Measurement Apparatus.....	11
5. Main Experiments and Findings	13
5.1. Experimental Apparatus and Setup	13
5.2. Flow Measurements.....	14
6. Discussion.....	18
6.1. Accuracy of the CFD Prediction	18
6.2. Summary comparison of performance.....	19
7. Conclusion	20
8. References	21
Copy of the Table of Contents of the Doctoral Thesis	22

SUMMARY OF THE DOCTORAL THESIS

1. Introduction

1.1. Motivation

Controlling the experimental environment is one of the key functionalities of closed-circuit wind and water tunnels. To achieve low levels of turbulence and a highly uniform velocity profile, wind tunnels traditionally rely on contractions upstream of the test section. Ocean basins, however, typically have a much larger test section relative to their return ducts (Fig. 1). This necessitates that the flow expands as it enters the test section, thereby decreasing flow uniformity and amplifying turbulence where it is least desired. Expansion turning vanes can be employed to alleviate some of these issues. However, prior to this project, suitable designs for water tunnels and ocean basins did not exist. Solving this issue became the main motivation behind this research.

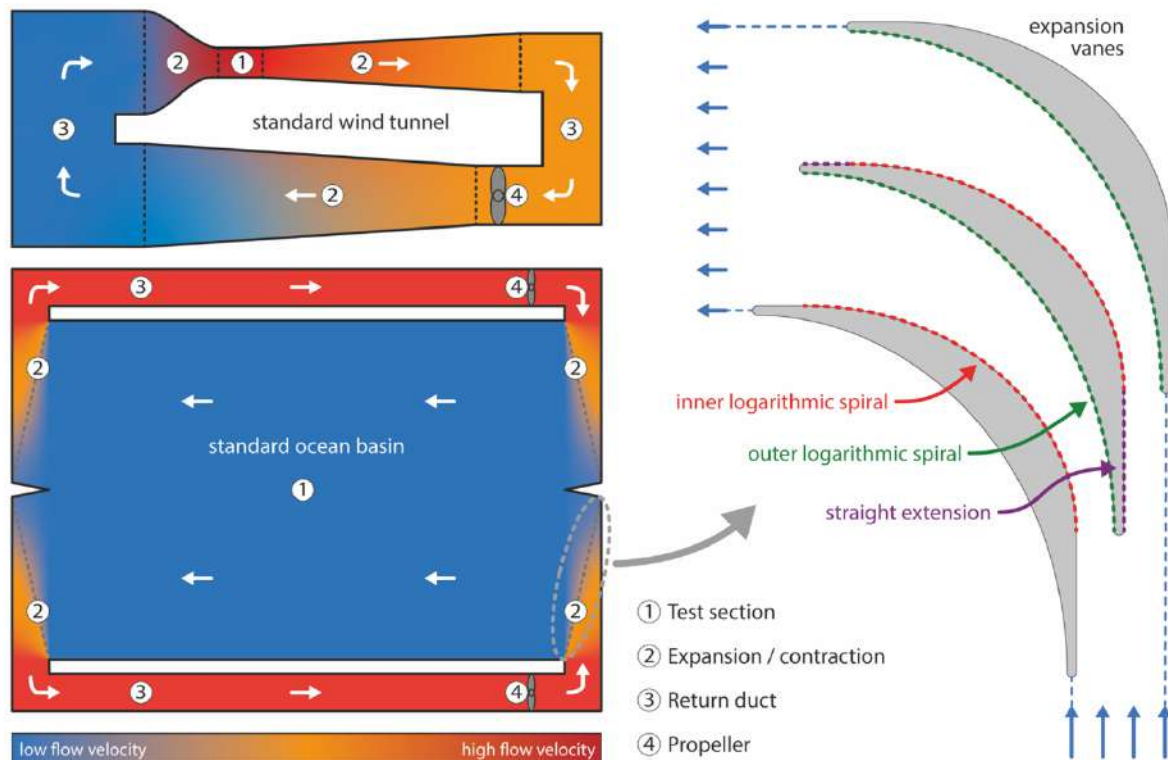


Fig. 1: Plan view of a typical wind tunnel (top) and an ocean basin (bottom), with an example of expansion vanes shown on the right.

1.2. Objectives and Purpose

The main objective of the doctoral research was to investigate the feasibility of turning vanes that simultaneously expand and turn the flow. These vanes will hereafter be referred to as *expansion vanes*. Once their feasibility had been established, their shape had to be optimised theoretically and experimentally.

To achieve these main objectives, various specific objectives had to be completed priorly. Firstly, the geometry of curved diffusers had to be parameterised to evaluate how the vane shape impacts the flow. Secondly, various simulations and physical experiments had to be conducted to optimise the shape of the expansion vanes. Next, a suitable testing environment

had to be set up, which had to be capable of creating the appropriate flow through the experimental expansion vanes. Lastly, the flow turbulence, flow uniformity, and pressure drop generated by the turning vanes had to be quantified and evaluated.

The purpose of the research was to improve the energy efficiency and flow uniformity of flow passing through an expanding corner. Of particular focus are expansion ratios of 1:2; as these large expansion ratios can often be found in water tunnels and current tanks.

1.3. Scientific Novelty

The research produced a novel profiled vane shape, which is significantly more effective at creating high-quality flow through an expanding corner than current standard flat-plate alternatives. Many flow tanks rely on excessively large motors that provide high flow quality by using a significant portion of the available power on flow-smoothing elements, such as honeycombs or wire screens. With the improved expansion vanes presented here, the need for such elements is lower and overall efficiency is increased. However, the new vanes require a more complex manufacturing process than simple flat-plate vanes and diffusers, thereby incurring higher associated costs.

2. Current State of Knowledge

2.1. Diffusers

To understand the limitations of expansion vanes, literature concerning diffusers is particularly helpful. Fundamentally, the work herein is based on a series of experiments conducted by Fox and Kline [1]. The researchers tested a range of curved diffusers with different effective expansion angles ($2\theta_{eff}$). Additionally, the size of the diffusers was normalised by taking the ratio of the length of the diffuser centre line (L) and inlet width (D_1). With an increase in expansion angle, a diffuser will exhibit one of four distinct stall behaviours as shown in figure 2.

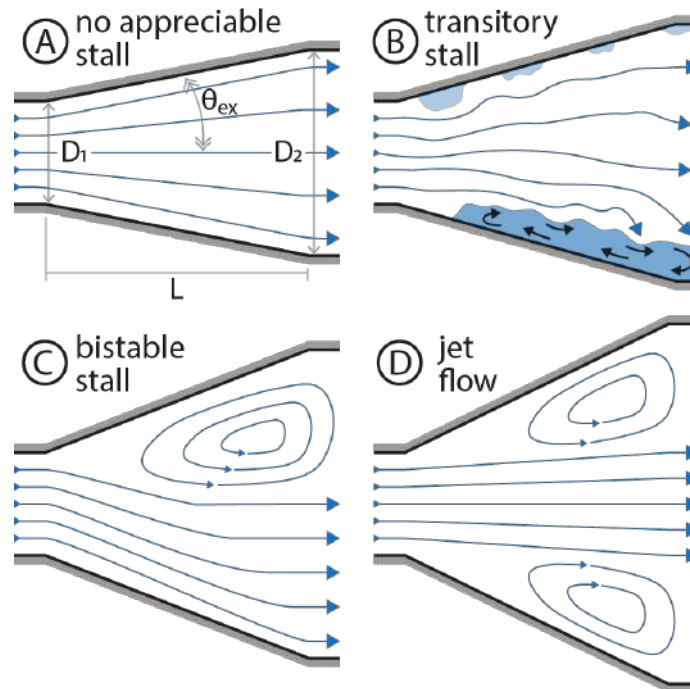


Fig. 2: Diffusers with varying expansion angles (θ_{ex}) and flow regimes [2]. Adapted from [3], [4], & [5]

Beyond standard diffusers, Fox and Kline also investigated curved diffusers. The researchers found that for turning angles (ω) of 30° or less, curved diffusers behave almost identically to their straight-walled counterparts. However, increasing the turning angle further moves the flow separation point further upstream. This amplifies the size of the flow separation, as illustrated in figure 3 [1].

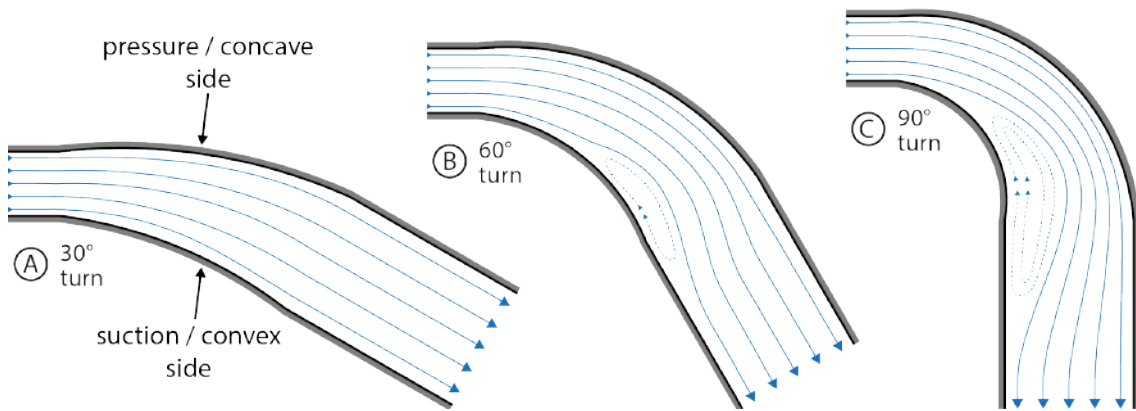


Fig. 3: Transitory stall regime in curved diffusers. The diffusers have the same expansion ratio and centreline length [2]. Adapted from [6].

To avoid high turbulence in testing facilities, diffuser stall and large flow separations are to be avoided. According to the data gathered by Fox and Kline shown in figure 4, it is impossible to size a curved diffuser with a turning angle of 90° and an expansion ratio of 2.0, while avoiding diffuser stall. However, the study only investigated diffusers with a circular arc centreline, akin to the left part of figure 8. The additional curvature control, built into the novel expansion vanes presented herein, allows for further optimisation.

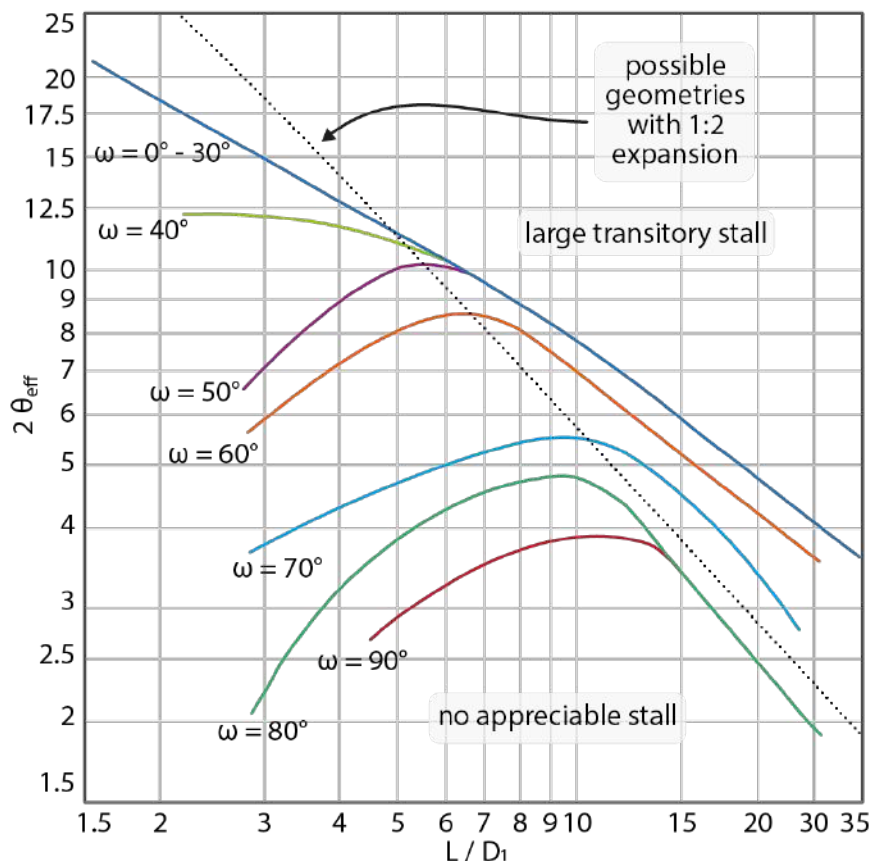


Fig. 4: Stall limits of curved diffusers at different turning angles (ω). Solid lines mark the lower boundary of the transitory stall region. Adapted from Fox et al. [1]

2.2. Expansion Vanes

Since Prandtl constructed the first closed-circuit wind tunnel, there have been extensive studies on turning vane cascades [7]. The advances in computational capabilities and the development of panel methods have allowed for further optimisation, as demonstrated by Sahlin and Johansson [8]. In recent years there has been renewed interest in the subject. If turning vanes are used to simultaneously turn and expand the flow, the footprint of wind tunnels can be significantly reduced. Such expansion vanes have been studied in detail by Lindgren et al. [9], as well as Lindgren and Johansson [10] [11]. Their designs find use in a wind tunnel at the Royal Institute of Stockholm (KTH).

The researchers found that they were limited to an expansion ratio of 1.5, above which cascade losses become unacceptable. A higher expansion ratio of 2.0 was achieved at MIT by Drela et al. [12]. Their concept combines turning vanes and dense wire screens to avoid flow separation and increase flow uniformity (Fig. 5). The design has been installed successfully in a novel wind tunnel at Brown University [13].

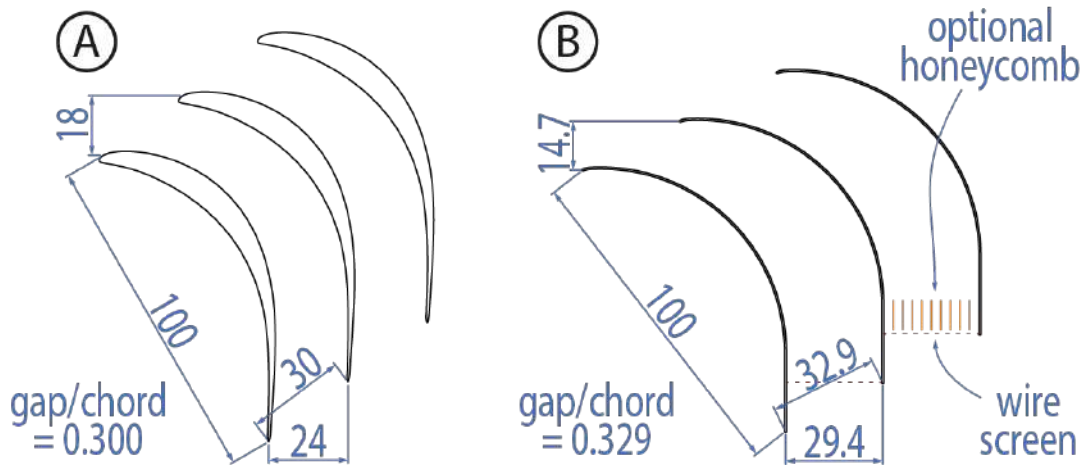


Fig. 5: Expansion vanes by Lindgren et al. (A) and Drela et al., (B). For comparison, the vanes are scaled to the same chord length [2].

Unfortunately, none of these designs are suitable for use in ocean basins or water tunnels. The KTH vanes offer an insufficient expansion ratio and the wire screen used in conjunction with the MIT vanes is too fine. When used in a water tunnel, the screen would clog up quickly during normal operation and access for clearing any blockage is usually very limited. The next sections will outline how a new type of expansion vane was developed, capable of achieving expansion ratios of 1:2 without the use of an internal wire screen.

3. Theoretical Contributions

Two different types of curved diffuser geometry are commonly mentioned in literature. The first is discussed in depth by Fox and Kline [1] and involves a centre-line arc with protruding spines to create the walls. The second method is described by Chong et al. [14] and is based on an inner and a central arc, which defines the outer wall. Unfortunately, both methods have certain disadvantages.

A straight wall diffuser does not provide a smooth transition to the straight channel walls at the inlet and outlet. While double arc diffusers have smooth transitions, their rate of expansion is inconstant. They have a low rate of expansion at the inlet which rapidly increases towards the outlet. In an attempt to overcome their shortcomings, a novel way of defining

curved diffusers was devised. Using logarithmic spirals as a basis, the designer gains precise control over diffuser expansion angle, turning angle and curvature distribution.

3.1. Developing the Theoretical Vane Shape

Logarithmic spirals can be manipulated to define the side walls of a curved diffuser. In a Python script written by the author, merely the coordinates and curve angles at the diffuser's inlet and outlet need to be specified. Assuming a 90° turning angle, a range of spirals is graphed in figure 6.

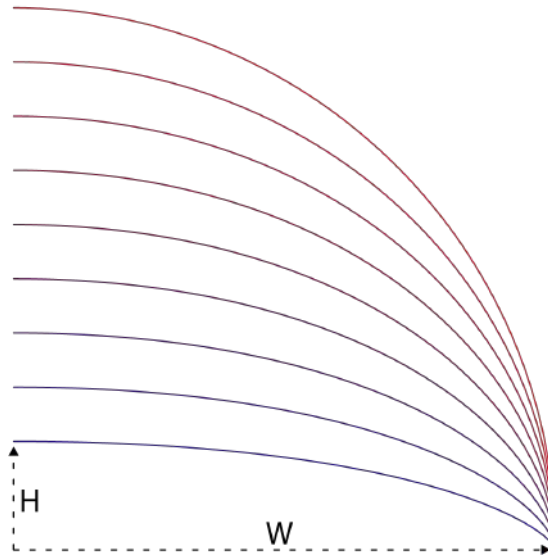


Fig. 6: Logarithmic spirals ranging from a H/W ratio of 0.2 (blue) to 1.0 (red) [15].

Here the inlet and outlet are at respective distances of W and H from the origin. The *stretch* of the spiral can be defined as the ratio of H/W . A stretch of one creates a curve equivalent to a circular arc, where the rate of turning is constant. A lower stretch has a higher rate of turning towards the inlet, while a larger stretch results in a higher rate of turning near the outlet. Once a suitable spiral has been found, it can form the inner or outer wall of a curved diffuser. The shape of this diffuser can then easily be adapted to form a suitable expansion vane. The outer and inner curves of the diffuser turn into the pressure and suction side of the vane respectively, as shown in figure 7. The designer also has to pay close attention to the gap-to-chord ratio. This is found by dividing the diagonal spacing of the vanes by the vane chord length.

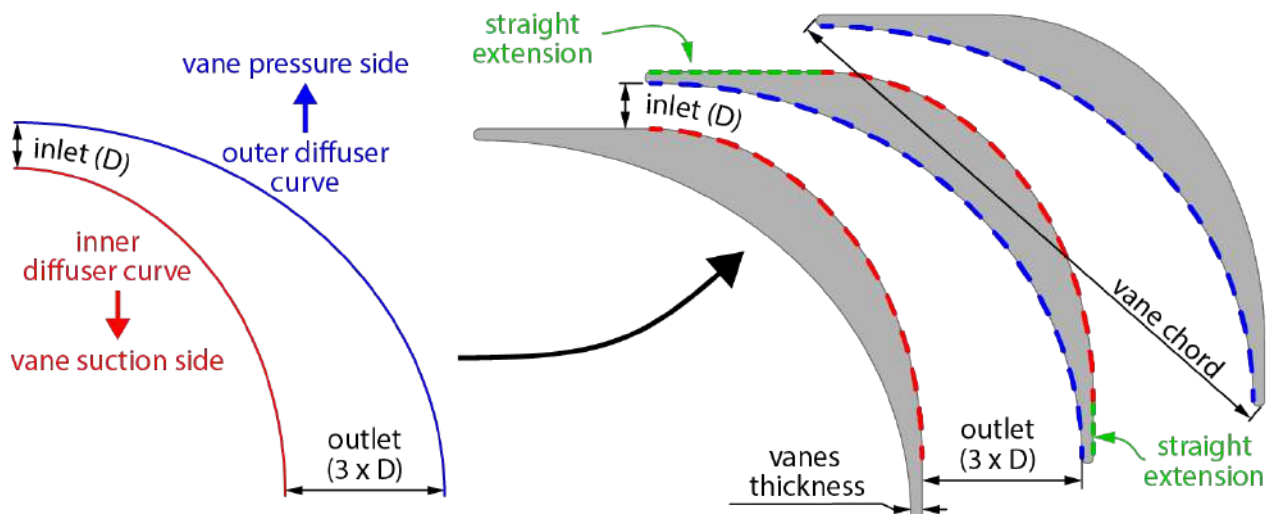


Fig. 7: Constructing a cascade of expansion vanes using logarithmic spirals [15].

As the vanes are created from logarithmic spirals, the designer has parametric control over the expansion ratio, turning angle and curvature distribution. The latter is controlled by varying the ratio of diffuser height and width (H/W). Here, a ratio of one signifies that the *centreline* of the diffuser is perfectly circular as shown on the left side of figure 8.

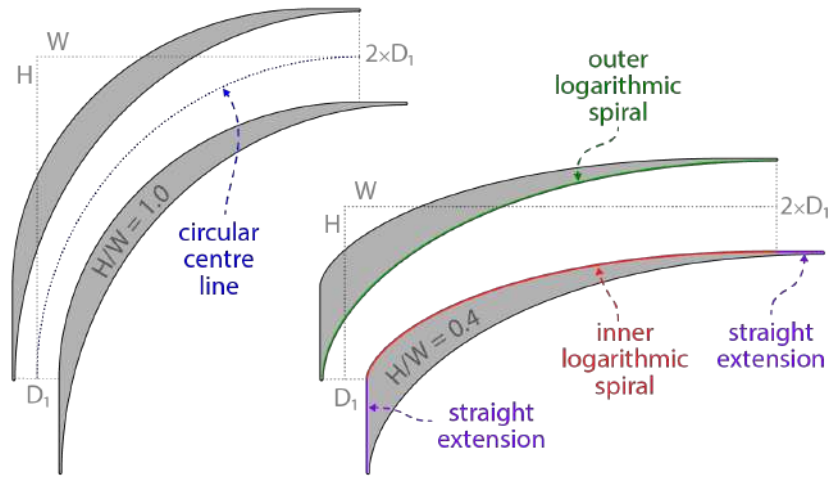


Fig. 8: Logarithmic vanes with an H/W of 1.0 and 0.4, a turning angle of 90° , and an expansion ratio of 2 [15].

3.2. Conducting CFD Simulations

Before carrying out physical experiments, various H/W ratios and numerous gap-to-chord ratios were investigated using computational fluid dynamics (CFD). The simulations were run on the open-source software package OpenFOAM, using the shear stress transport $k-\omega$ (i.e., SST $k\Omega$) turbulence model. Due to the computational resources available for this investigation, simulations were carried out in two dimensions only. Using turbulence modelling and ignoring the three-dimensionality of the flow clearly reduces the accuracy of the solution. However, as the CFD results merely serve as a starting point for real-world experiments, this compromise was deemed acceptable.

The boundary conditions for the vane simulations were carefully defined to achieve maximum accuracy. Instead of simulating an entire vane cascade, only a single vane channel was simulated, as shown in figure 9.

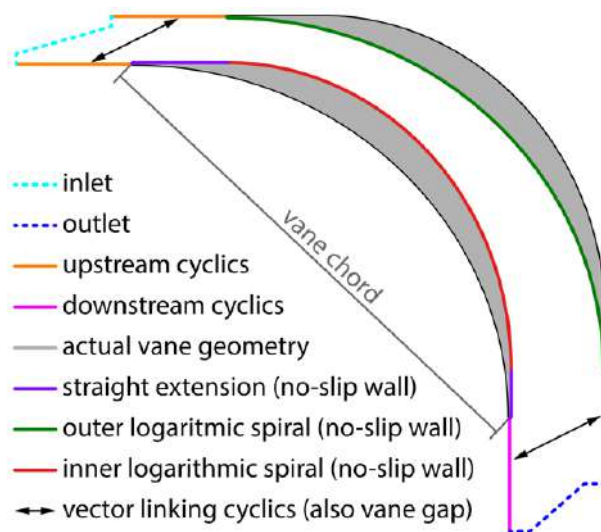


Fig. 9: Boundaries used in CFD simulations. The cyclic boundaries are not to scale.

Cyclic boundaries were placed upstream and downstream of the channel. These boundaries come in pairs which are coupled through a user-specified vector. If flow crosses a cyclic boundary it is transported to the corresponding location on its partner and vice versa. This simple setup allows for the approximation of an infinitely long cascade of vanes, while only simulating a single vane channel.

The inlet and outlet have somewhat peculiar shapes to ensure perpendicularity with the cyclic boundaries. This allows for better mesh snapping in the corners, which in turn ensures that the cyclic boundaries can be coupled more accurately. The surface of the vanes is modelled as a standard non-slip wall. The inlet spacing used for these simulations was set at 18mm. The domain was extended by 25 and 40 inlet widths upstream and downstream respectively. The CFD simulation examined three main characteristics:

- Turning angle – Ideally the flow is turned through 90°. Any deviation from this value would mean that the flow is not aligned with the channel downstream of the turn, thereby decreasing flow uniformity
- Flow uniformity – Quantified using the coefficient of variation. A coefficient of variation close to zero would indicate uniform flow which is highly desirable in wind and water tunnels.
- Energy requirements – Measured based on the loss factor K . Essentially this is the energy through a flow conditioner as a ratio to the kinetic energy per unit volume in the flow, as shown in equation (1) [16].

$$\Delta p = \frac{1}{2}K\rho u^2 \quad (1)$$

The first set of simulations attempted to find the most suitable H/W ratio. Initial guesses on gap-to-chord ratios and expansion angles were based on the aforementioned findings of Fox and Kline. In total, eight different H/W ratios, ranging from 0.4 to 1.1 were tested on two expansion vane geometries with different gap-to-chord ratios. These tests showed that a H/W of 0.7 offered the best performance.

For the subsequent experiments, the H/W ratio was fixed at 0.7. Next, nine different gap-to-chord ratios, ranging from 0.143 to 0.290, were investigated. These simulations showed that a gap-to-chord of 0.230 offered the best compromise of flow uniformity, turning angle and loss factor. After a suitable vane shape had been determined, the first vanes could be manufactured.

4. Practical Contributions

4.1. Constructing the vanes

Once the vane shape had been optimised theoretically in CFD, it had to be recreated physically. To this end, the vanes were digitally modelled in SolidWorks. The model was then imported into Cura, a slicing software that converts models into instructions for 3D printers. These instructions were then passed to a Creality Ender 6 Core-XY printer. All components were printed in PLA at a nozzle temperature of 210°C and a heated bed temperature of 60°C. The nozzles used were 0.4mm in size and the layer height was usually set at 0.12mm. Both the logarithmic vane shape and the geometry developed at MIT were tested. The latter was included as a benchmark.

4.1.1. Printing and Assembling the Logarithmic Vanes

Early prototypes, attempted to print the vanes in one 300mm piece. However, with increased model height, the adhesion of the vane to the print bed degraded. Usually, a single layer of support material around the bottom edge of the print, known as a brim, can be used to increase adhesion. Unfortunately, in this case, increasing the brim size did not bring about the desired effect. The prints kept separating thereby making the resulting vane unusable. To overcome the adhesion problems, it was decided to print the vanes in two halves, one male and one female part. These pieces could then be joined using a combination of press fitting and applying additional adhesive

The final design of the logarithmic vanes had a wall thickness of 0.8mm which is equivalent to a double track using a 0.4mm nozzle. A central reinforcing rib was slightly thicker and measured 1.2mm. For the female part of the pair, the rib terminates 20mm below the top. This avoids clashing with the extension of the male part. Adequate adhesion is provided by a single-layer 8mm brim at the base of the vane and the brim was removed after printing using a standard deburring tool (Fig. 10).

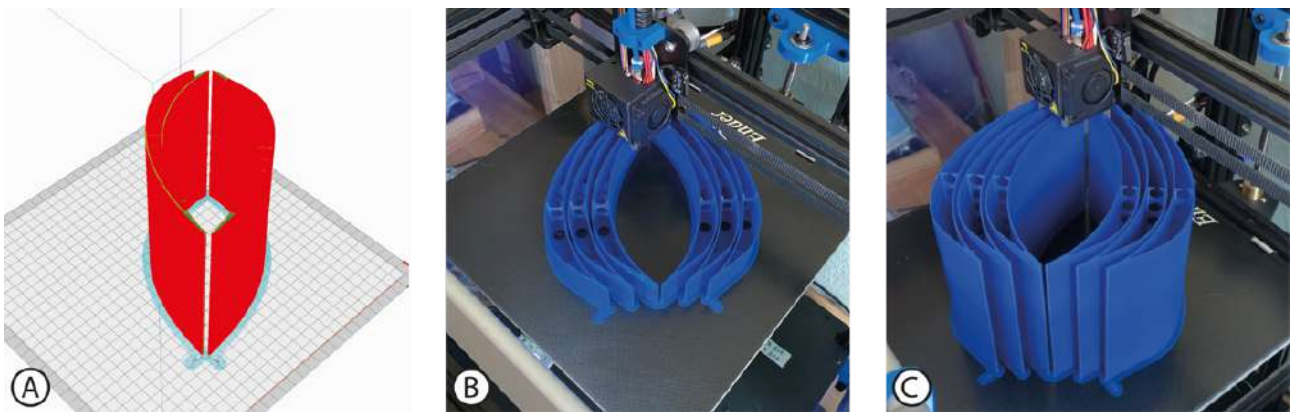


Fig. 10: The vane geometry as shown in Cura slicing software (A), the beginning of vane print (B), and the final stages of vane print (C).

For assembly, the female halves were bolted to a metal side plate using M10 bolts and an internal female thread. Next, the male parts were slotted into position. Then, the second side wall was bolted onto the vane cascade. Four M6 threaded bars were fed through the assembly to ensure everything was clamped together rigidly. Cyanoacrylate adhesive was used to align the trailing edge of the vanes in a few locations where they did not line up perfectly (Fig. 11).



Fig. 11: Vanes being mounted to the side wall (A), a vane pair being joined (B), and the fully assembled vane cascade with bolted connections clearly visible (C).

4.1.2. Printing and assembling the MIT expansion vanes

The MIT vanes, essentially thin flat plate vanes, were printed with 100% infill to make them as durable as possible. Their thin cross-section would not have allowed for sufficient print bed adhesion on its own. It was therefore decided to print them in pairs with a connecting base plate. The opposite end of the vanes would be closed using a separately printed end plate with dedicated slots for the vanes. As this type of vane is not hollow, a male-female join at the centre of the channel could not be incorporated. Fortunately, the base plate offered adequate print bed adhesion for the vanes to be printed to their full 305mm height (Fig. 12).

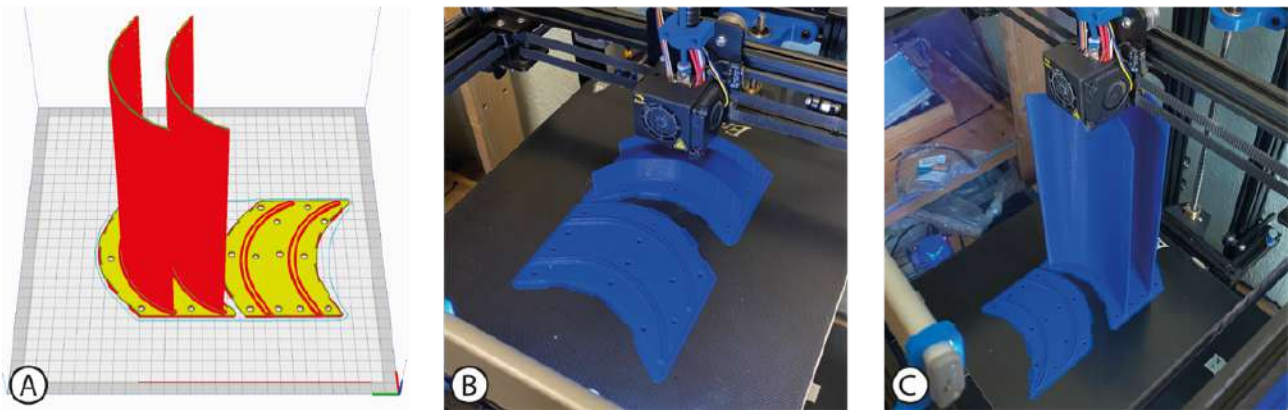


Fig. 12: Vane geometry as shown in Cura slicing software (A), start of vane print (B), final stages of vane print (C).

Originally, the MIT vanes were designed to incorporate wire screens, spanning the gap between vanes at their trailing edge. For this project, instead of using wire screens, perforated plates were 3D-printed with small tabs that would sit in dedicated slots in the vanes, as shown in part A of figure 13. While the perforated plates have the same ratio of the open-to-blocked area as the original wire screens, the size of the individual holes has been increased. This was done to prevent the screens from clogging up if they were to be used underwater.

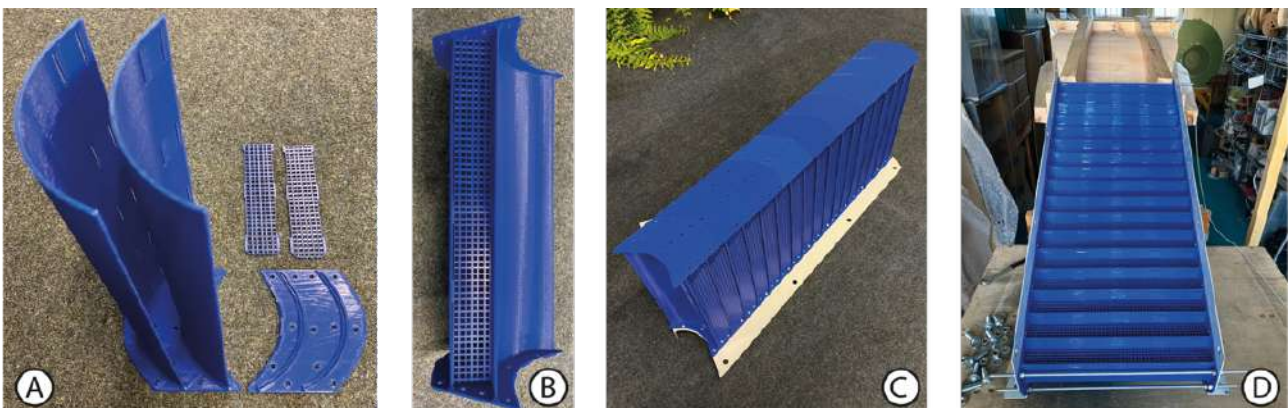


Fig. 13: Components for MIT vane pairs (A), assembled vane pair (B), cascade with a side wall (C), and fully assembled vane cascade attached to contraction (D).

To make room for these slots, the straight trailing edge section of the vanes was extended by 5mm. The original intention was to have interchangeable perforated plates with varying porosities. Unfortunately, the vanes proved too fragile to hold the screens without adhesive. In fact, initial tests using these vanes without the screens resulted in multiple fatigue failures at the base of the vanes and at the corners of the slots. These were likely caused by excessive vibration at higher flow velocities. This issue could be fully mitigated by glueing the screens in place.

For future experiments, it would be advisable to construct the vanes without the trailing edge extension and fix the screens in place from the beginning. The vanes are fixed to the side walls using M4 button head bolts and nuts, the latter being located outside the side wall. Four additional M6 threaded bars (two at either end) are used to pin the entire structure together.

4.2. Constructing a Wind Tunnel

To ensure the experiments were conducted in an excellent testing environment, a wind tunnel was constructed specifically for this doctoral research project. Drawing from his years of experience in the wind and water tunnel industry, the author designed and built every section of the machine (Fig. 14). After construction, every component was tested individually to ensure high flow uniformity and low levels of turbulence.

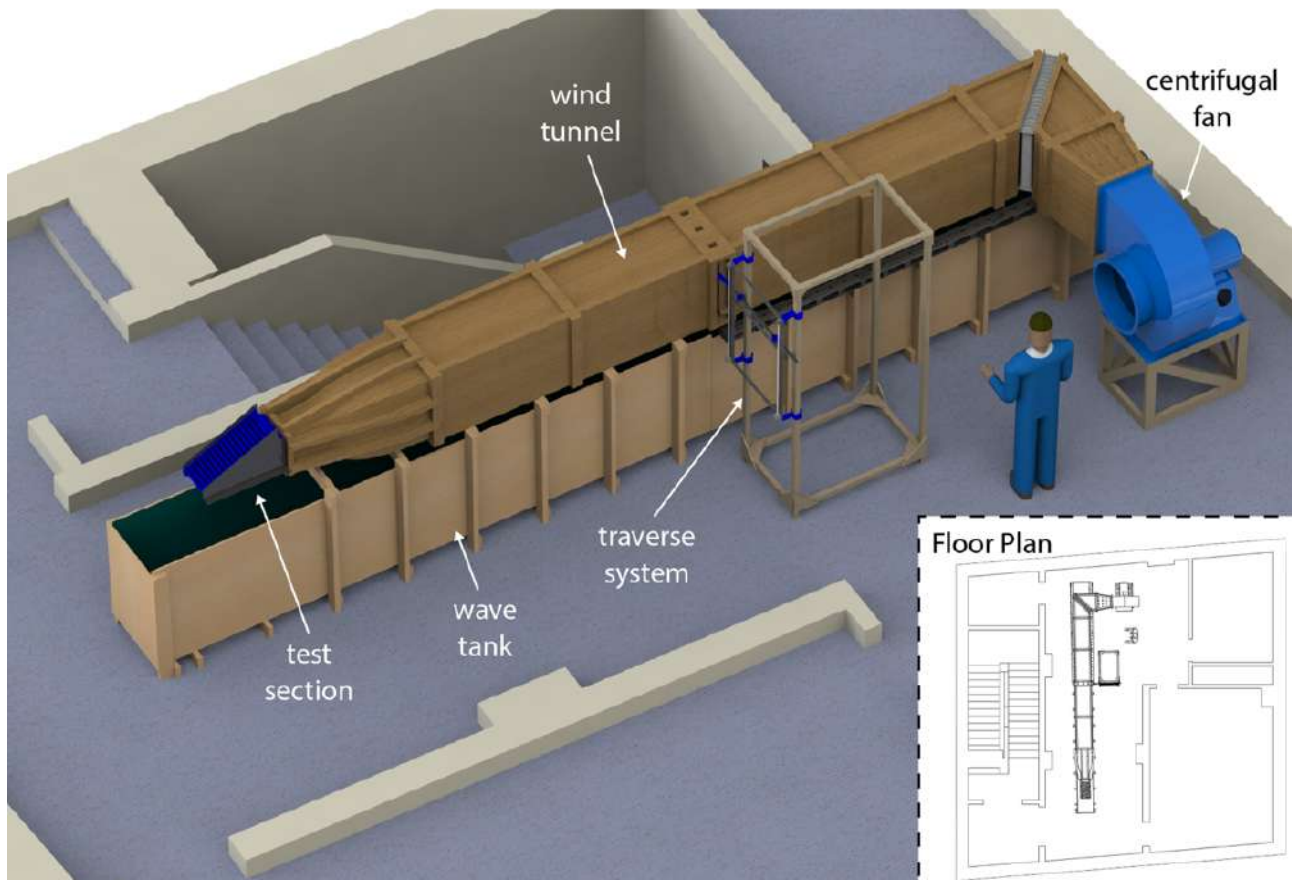


Fig. 14: 3D SolidWorks rendering of the wind tunnel. The person shown is 183cm tall and the walls have been cropped to enhance clarity [17].

The majority of the tunnel was constructed using UK standard wood, where plywood sheets measure 2440 x 1220mm. Material wastage was minimised by adopting a wind tunnel cross-section of 600 x 600mm and setting the length of most sections at approximately 1200mm. This resulted in a tunnel of sufficient size and reduced material cost.

4.3. Constructing the Measurement Apparatus

After some initial evaluation of various measurement techniques, it was found that using a seven-hole probe provided a good trade-off between cost and measurement accuracy [18]. To obtain a statically converged velocity reading in the wind tunnel, the seven-hole probe needed to remain in the same position for approximately 5 seconds. For several experiments, it was desirable to map the flow across the entire cross-sectional area of the wind tunnel, which

required several hundred distinct points of measurement over several hours. It was therefore unfeasible to accurately move the probe to all these locations by hand. To overcome this issue, a traverse system was constructed from aluminium extrusions, printed components and parts from a used Ender CR-10 3D printer (Fig. 15).

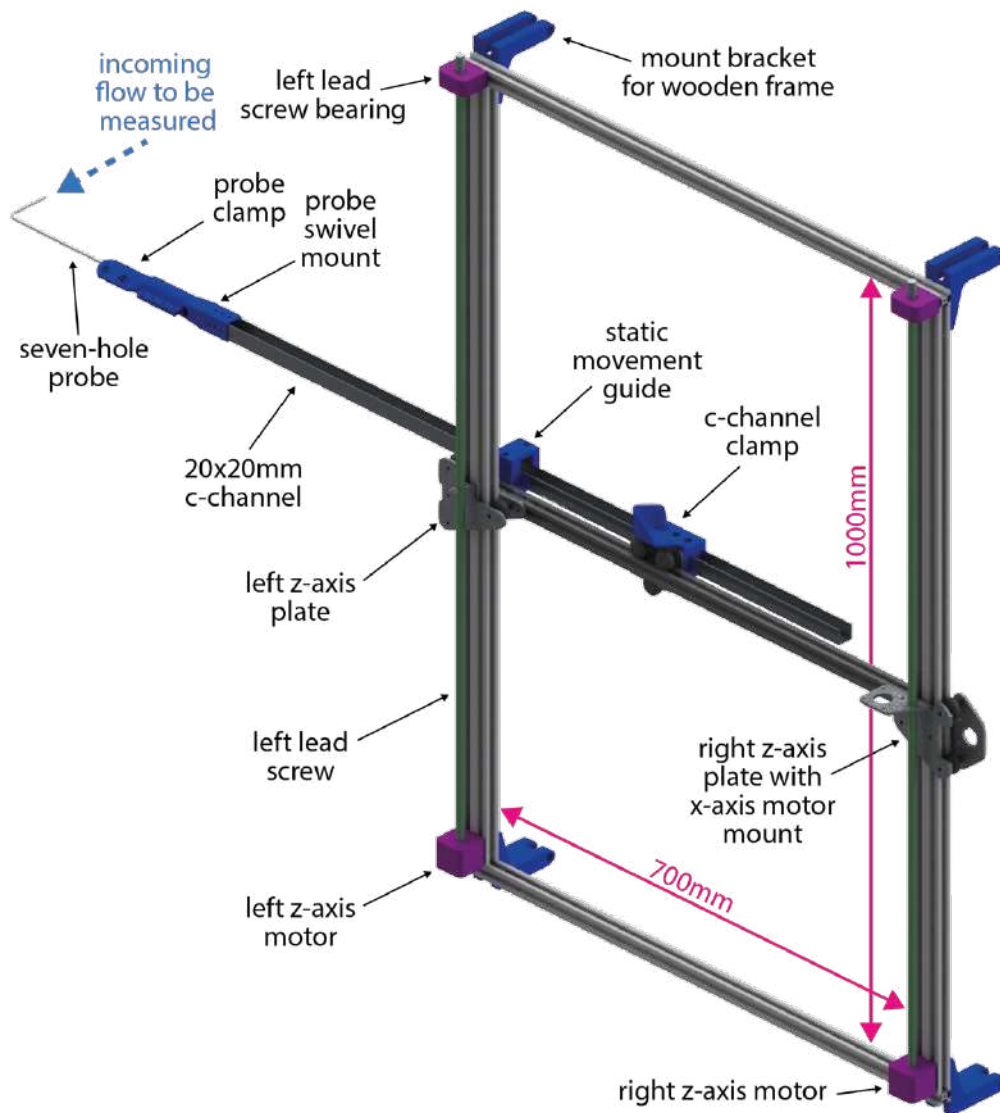


Fig. 15: Traverse system, used to automatically and accurately move the pressure probe to predefined locations.

Building the traverse system around 3D printer parts had several advantages. The printer's motherboards could be used to interface with the traverse system and existing software could be employed to control its motion. Finally, 3D printers usually have sub-millimetre accuracy, which is more than adequate for a traverse system of this kind. To measure the flow, a seven-hole probe was mounted on the traverse system. The system was supplied with 3D printer instructions but positioned a seven-hole probe instead of a print head.

5. Main Experiments and Findings

5.1. Experimental Apparatus and Setup

The physical experiments to characterise the expansion vanes were carried out in a purpose-built open-circuit wind tunnel. The machine is powered by an 18.5kW centrifugal fan, capable of supplying $4\text{m}^3/\text{s}$ of airflow at a pressure of 3000Pa. The fan is followed by a five-meter-long settling chamber, with a cross-section of 600 by 600mm. Various wire screens and a honeycomb ensure low levels of turbulence and secondary flow. Downstream of the settling chamber, a contraction section further improves the quality of the flow. The contraction was shaped in accordance with a 2002 publication by Lindgren and Johansson [10]. Its final cross-section measures 305 by 305mm, resulting in a contraction ratio of approximately 4:1.

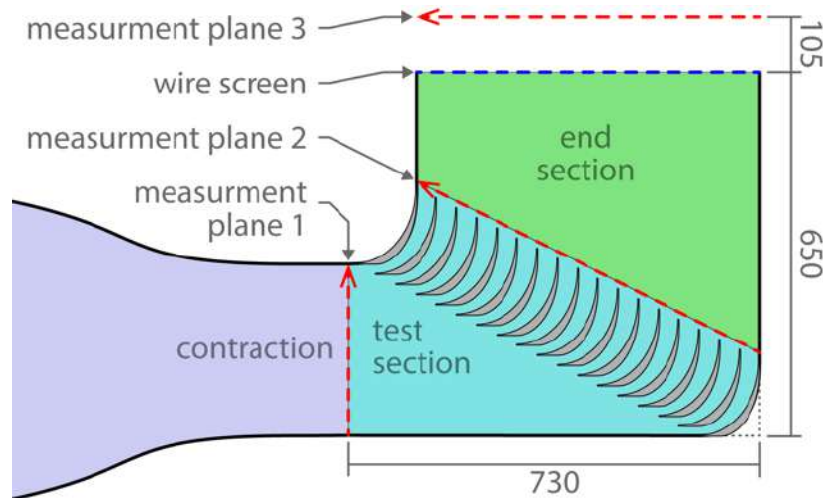


Fig. 16: Cross-section of the wind tunnel exit (lengths in mm)

Figure 16 shows the general setup for characterising flow through the expansion vanes. Measurement plane 1 corresponds to the end of the contraction, where the flow is comparatively uniform and contains little turbulence. The test section can be bolted to the end of the contraction to measure the flow immediately downstream of the vane cascade along plane 2. An end section can be installed to see the impact of constraining the flow downstream of the vanes, measured along plane 3. The red arrows indicate the direction of the measurement coordinates. The removable external wire screen has a wire thickness of 1mm and a uniform pitch of 4mm.

Flow measurements were conducted using a seven-hole probe paired with a multichannel pressure scanner. The probe incorporates a static pressure ring for accurate reference pressures. The scanner uses a board with eight slots for pressure-sensing cards. Each card supports eight pressure measurement channels. The cards have a measurement accuracy of 0.25% of their measurement range. The scanner used herein is equipped with 160Pa, 1000Pa, and 4000Pa cards. During flow testing, the cards were chosen to maximise measurement accuracy. Both the probe and the scanner were supplied by Surrey Sensors. To guarantee a statistically converged velocity reading in the wind tunnel, the seven-hole probe remains in the same position for approximately five seconds. Grids of measurement points give an accurate characterisation of the flow upstream and downstream of the vane cascade.

5.2. Flow Measurements

Four separate configurations of vanes have been assessed: the plain MIT vanes, the plain logarithmic vanes, the MIT vanes with the built-in screen, and the logarithmic vanes with an external wire screen at the outlet of the end section (Fig. 16). The performance of each configuration was compared to determine their effectiveness.

5.2.1. Measurements downstream of the contraction

To ensure that the vanes were tested in an adequate environment, the flow downstream of the contraction has been characterised using a 21x21 measurement grid. The glyphs in figure 17 indicate the location of the individual measurements.

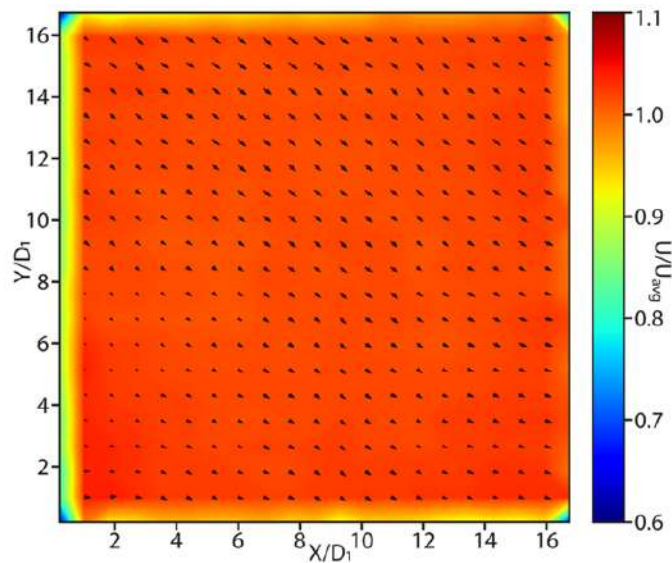


Fig. 17: Vertical velocity contour immediately downstream of the contraction (plane 1). U_{avg} is 44m/s

At a uniformity index of 0.986, the velocity contour is clearly very even. Furthermore, the turbulence intensity is merely 0.5%. There is a slight secondary flow to the right, which is likely to be encouraged by the position of the centrifugal fan. However, the magnitude of the secondary flow is below 2.5% of the primary velocity magnitude. Therefore, it should have a negligible impact on the flow results and analysis. The flow speed in this particular test was approximately 44m/s, though an additional test at 25m/s yielded very similar results, indicating the inlet conditions are adequate at all test speeds used herein. With the test section inlet conditions fully characterised, the expansion vanes and their performance could be tested and evaluated.

5.2.2. Measurements at the trailing edge of the vanes

Given the highly uniform and symmetric flow profile downstream of the contraction, the flow downstream of the expansion vanes is expected to be fairly symmetric as well. Therefore, the flow behind the expansion vanes was only measured over half the channel, and the resulting contours are shown in figure 18.

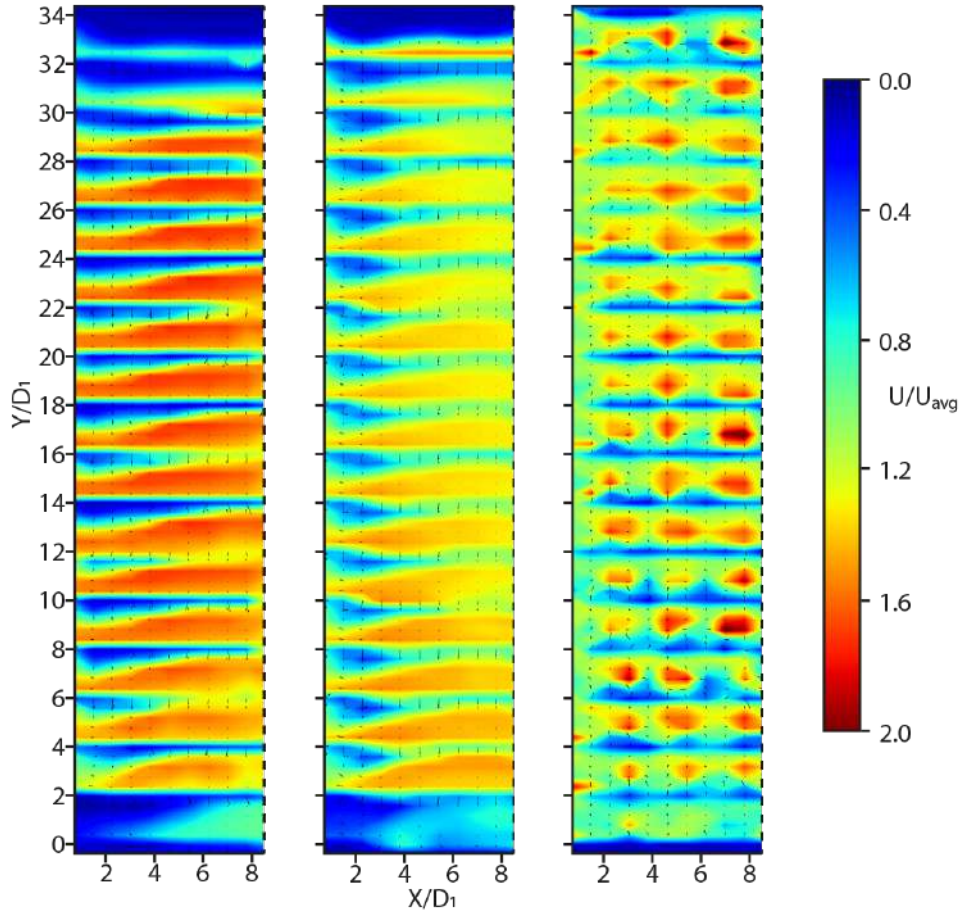


Fig. 18: Diagonal velocity contours (plane 2) at the trailing edges of MIT vanes (left), logarithmic vanes (centre) and MIT vanes with internal screens (right). U_{avg} is 20m/s

While measurements were taken diagonally along measurement plane 2, the coordinates used are projected from plane 3. The measurement grid was 11 by 88 points, which equates to 5 points per individual vane channel. The centreline of the channel is indicated by the dashed lines.

In this comparison, the highest quality flow is achieved by the MIT vanes with the internal screen. However, the probe is apparently too close to the screen, leading to localised regions of fast jet flow, where the probe coincidentally lines up with holes in the screen. Measurements further downstream will be discussed in a subsequent section. At first glance, even without an internal screen, the MIT vanes seem to outperform the logarithmic vanes, having a slightly higher uniformity, and approximately the same pressure loss factor (exact quantities are shown in Table 1). However, during testing, a regular swoosh could be heard coming from the MIT vanes. In order to investigate the source of this noise, the flow probe was moved to the centre of the channel and the flow was measured at various fan speeds.

5.2.3. Oscillating flow downstream of the vanes

The previous velocity contours show the time-averaged velocity over 5 seconds at each point, which potentially hides flow unsteadiness that might occur over shorter timespans, thereby giving a false impression of steady flow. However, figure 19 clearly shows severe periodic unsteadiness in the flow through the MIT expansion vanes. Therefore, it is no surprise that this configuration has the highest level of turbulence intensity of any tested configuration (additional turbulence intensity values are shown in Table 1).

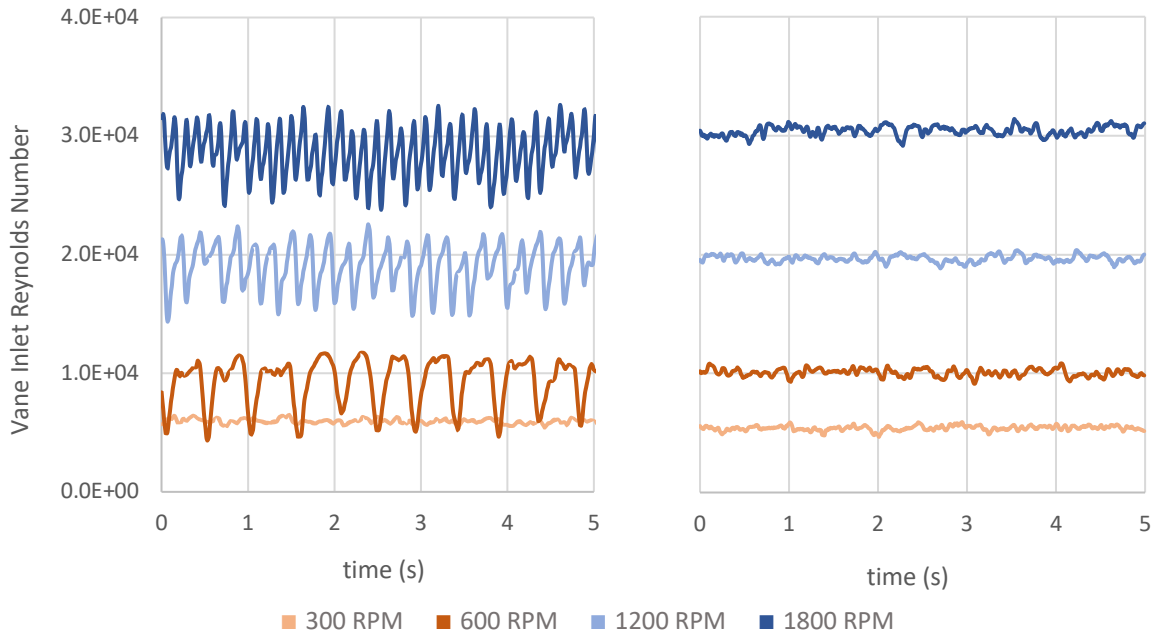


Fig. 19: Velocity measurements for the screenless MIT vanes (left) and screenless logarithmic vanes (right) at the indicated fan speeds, measured at the centre of plane 2

The oscillations set in above a vane-inlet-based Reynolds Number of 10,000. Despite their comparatively high uniformity index, the flow unsteadiness along with the high turbulence intensity disqualify the screenless MIT vanes from being used in flow research facilities. Unfortunately, the problems related to unsteadiness do not end here. The flow through the logarithmic vanes also exhibits some unsteadiness, but only when the end section is installed. Therefore, a brief investigation into possible causes was conducted.

After various trial and error modifications, it was discovered that strong oscillations can be created by partially obstructing the innermost channel of the vane cascade. This was achieved by taping over the central 183mm of the 306mm channel. Installing the end section, causes oscillations to set in at a Reynolds Number of 30,000, while obstructing the innermost channel lowers this threshold to approximately 15,000, as shown in figure 20. The oscillation in the logarithmic vanes can be entirely suppressed by installing a wire screen downstream of the end section. It is believed that a lack of flow through the innermost channel leads to these oscillations, and they might be closely related to diffuser stall, although further investigation is needed. A possible solution might be to design a vane cascade with a lower expansion ratio for the innermost channel.

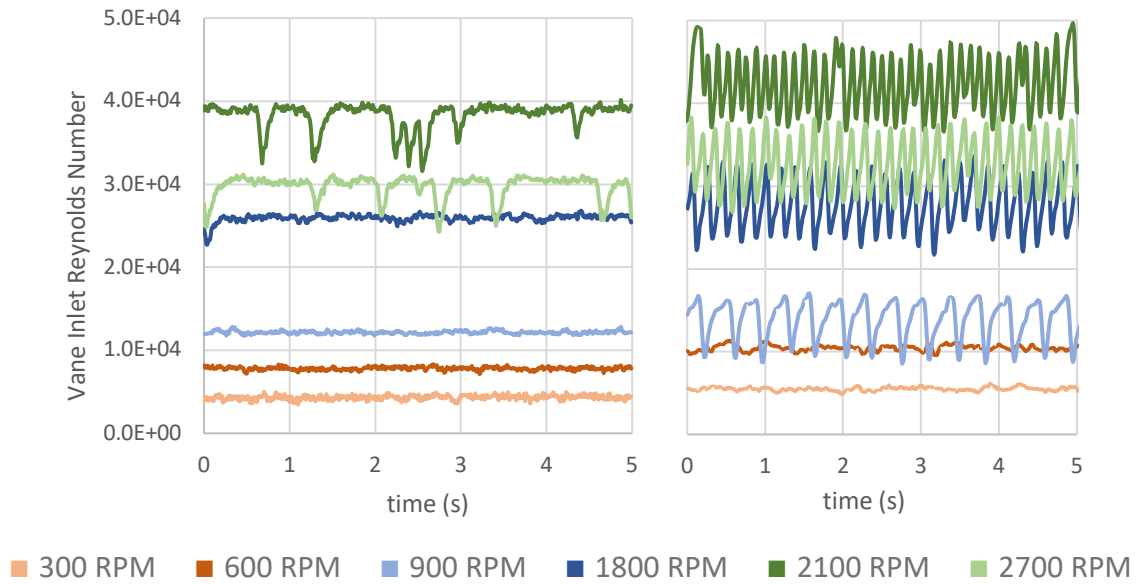


Fig. 20: Velocity measurements for the logarithmic (top) and logarithmic vanes with the innermost central channel partially blocked (bottom) at the indicated fan speeds, measured at the centre of plane 3 (end section installed)

5.2.4. Measurements downstream of the end section

In light of the oscillations observed downstream of the screenless MIT vanes and issues with their fatigue strength, this configuration was not fully characterised downstream of the end section. Some preliminary trial runs indicated a flow profile very similar to that of the screenless logarithmic vanes, shown in figure 21.

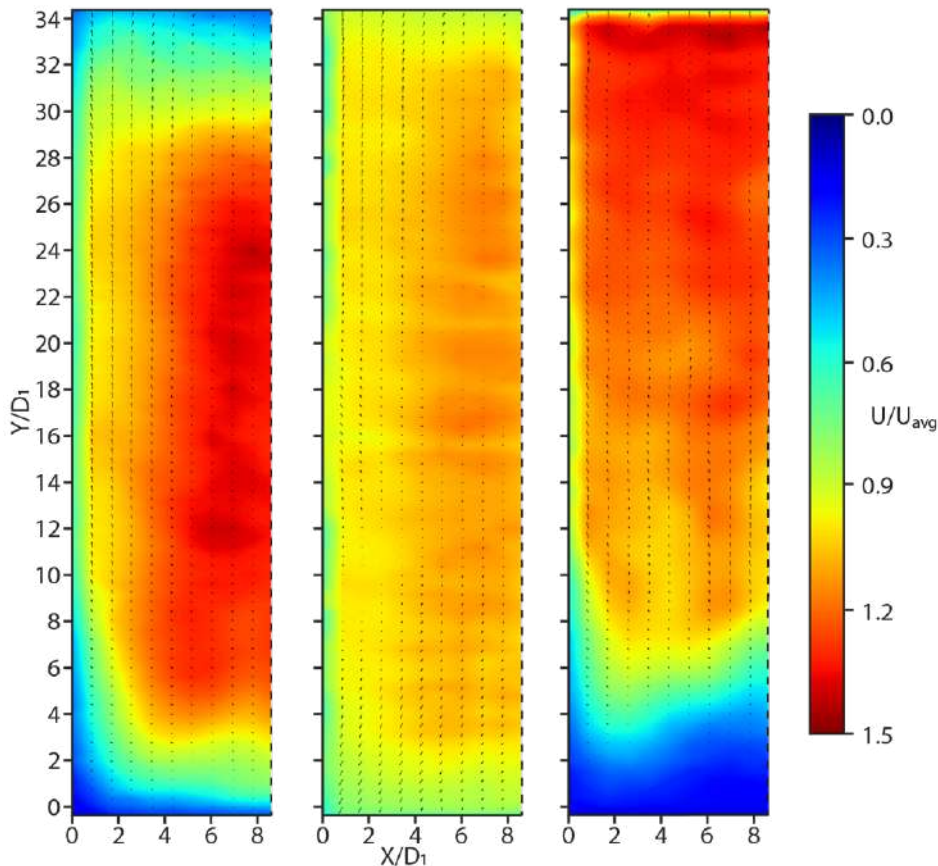


Fig. 21: Velocity contours downstream of the end section (plane 3) of the logarithmic vanes without (left) and with a wire screen across the end section (centre), as well as the MIT vanes with internal screens (right). U_{avg} is 19m/s

The screenless logarithmic vanes seem to have some flow deficiencies in the corners of the channel. This is especially severe downstream of the outermost vane, in line with coordinate 0, 0. These results somewhat match the findings of Drela et al. [12]. The flow deficiency in this particular location is caused by a larger boundary layer upstream of the vanes, which in turn is generated by the longer side wall.

The logarithmic vanes, in combination with a wire screen covering the end section, offer a viable alternative. The flow is aligned with the channel and the smoothing effect of the wire screen yields a highly uniform flow. The uniformity index is about 11% higher downstream of the logarithmic vanes with the external screen than it is downstream of the MIT vanes with the internal screen.

As shown in figure 18, the flow immediately downstream of the MIT vanes is comparatively uniform, though artefacts from the screen clearly impacted measurements. By the time the flow reaches measurement plane 3, it has travelled between 315 and 615mm, which is equivalent to a minimum of 79 screen hole diameters. At this point, the individual jets generated by the screen holes should have dissipated completely and flow uniformity should be higher. However, when examining figure 21, it is clear that Uniformity has decreased. The original MIT publication stated that their expansion vanes turn the flow by approximately 90°. These findings could not be replicated with the geometry used herein, which turns the flow through 117°. This overturning leads to a misalignment between the flow and the wind tunnel channel, causing an area of high velocity near the inside of the turn and flow deficiency on the opposite side. As aforementioned, the MIT vane geometry has been altered. The trailing edge was extended, thereby lengthening the vane chord by 3.5%, while the screen was coarsened by 12,200%. As the change in screen hole dimensions was much more substantial, the author suspects that the screen is more likely to be the source of the flow overturning. This theory is supported further by the lack of overturning prior to the installation of the internal screen. Nevertheless, more research is required to confirm this theory.

6. Discussion

6.1. Accuracy of the CFD Prediction

A detailed flow profile measurement was taken across the middle of the central logarithmic vane channel and the results were compared to the CFD simulations of the same expansion vane geometry. As shown below (Fig. 22), there is a decent agreement between the experimental and simulated results of the velocity profile.

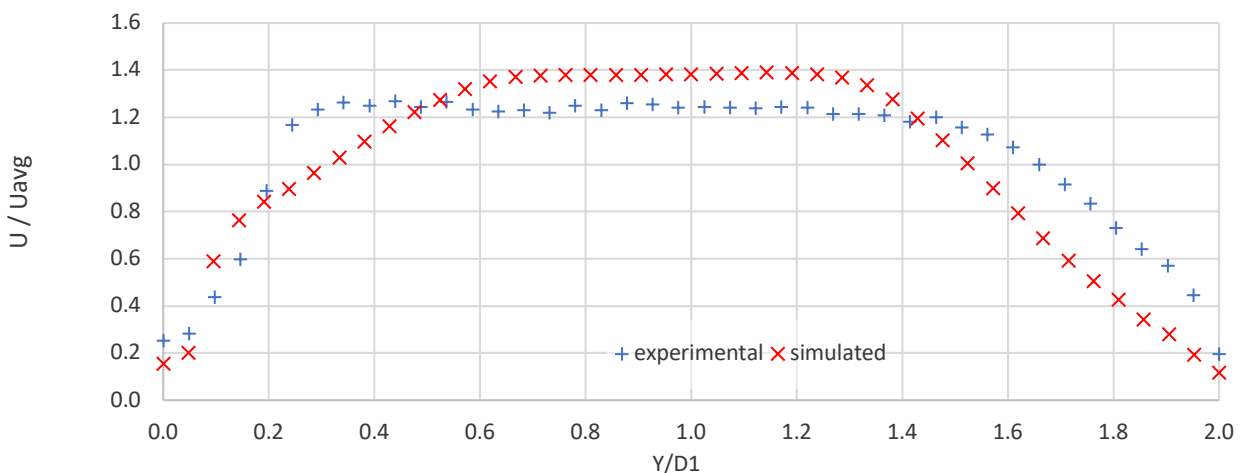


Fig. 22: Detail flow profile across a single vane channel created using experimental and simulated data

Evidently, the flow deficiencies along the channel walls are more pronounced in the simulation compared to the real-world results. This is a positive surprise, as the physical vanes produce a more uniform flow than expected. Furthermore, the CFD significantly underpredicted the loss factor. There are numerous possibilities that might have led to these discrepancies:

- Turbulence in the simulation is modelled, not resolved. The research budget imposed computational constraints and the turbulence had to be modelled using RANS solvers instead of resolving individual eddies using LES solvers.
- The simulation was set up as a 2D model, which negates any secondary flow effects. The physical experiments clearly show that the flow is highly three-dimensional.
- The simulated inlet was assumed to be perfectly uniform. While the experiments strived for maximum uniformity, the proximity of the walls and other vanes in the cascade inevitably led to small disturbances.

For future research, it might be beneficial to investigate which factors contribute most to the discrepancies. Better simulations allow for more accurate prediction, which might enable further increases in efficiency.

6.2. Summary comparison of performance

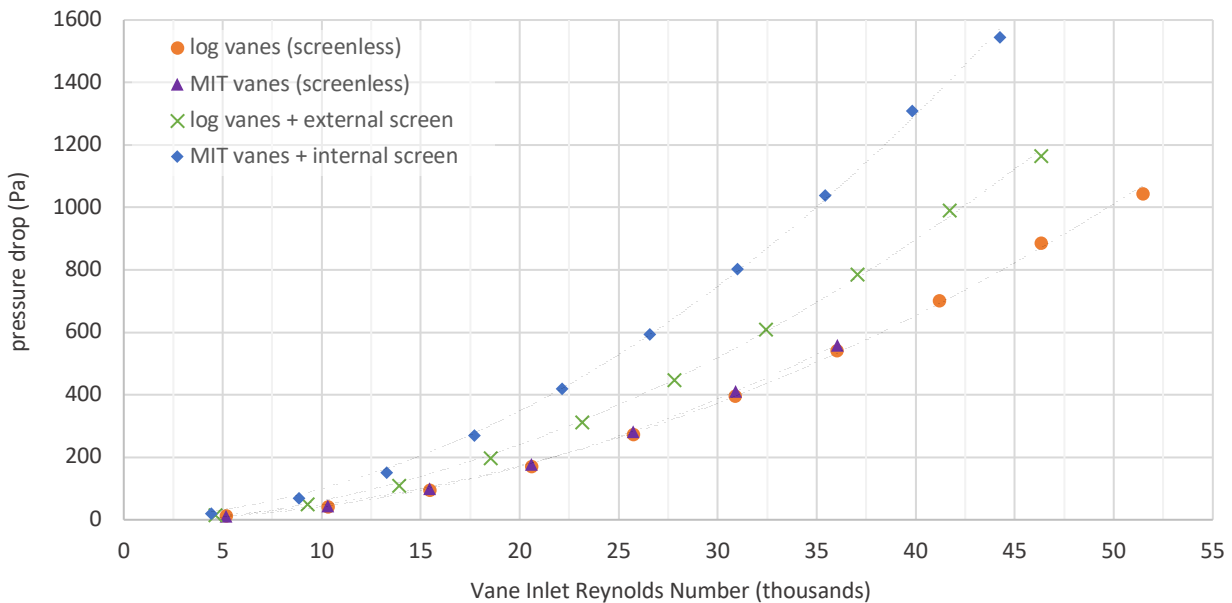


Fig. 23: Pressure drops for logarithmic vanes and MIT-style vanes with and without screens

As demonstrated by figure 23, the lowest pressure drop is generated by the vanes without screens, where both the logarithmic and the MIT vanes perform very similarly. Introducing an external screen downstream of the logarithmic vanes leads to an increase in pressure drop in the system. The highest pressure drop is generated by the MIT vanes with the integrated screens, which have significantly higher losses when compared to the logarithmic vanes with external screens. The difference in pressure drop between the logarithmic vanes with and without the external screen is in line with pressure loss measured across the wire screen by itself. All line fits are second-order polynomials with exceptionally good R^2 values of 0.999 or higher.

A summary of the flow characteristics of the various flow experiments is shown in Table 1. The “plane” column refers to the measurement planes shown in figure 16. The MIT vanes

with an internal screen have the highest flow uniformity in measurement plane 2. However, as the installation of the internal screen leads to an overturning of the flow, the uniformity degrades sharply by the time the flow reaches measurement plane 3. At this location, the best performance is achieved by the logarithmic vanes in combination with the additional external screen. This configuration also has the advantage of a 4.1% lower loss factor. Should flow uniformity be of lesser interest, it would be best to choose the screenless logarithmic vanes as they have a low loss factor, but, unlike the screenless MIT vanes, they also deliver steady flow.

Table 1: Flow quality indicators for different vane configurations and locations

Test	plane	screen	CV	γ_{L1}	I	u_{avg} (m/s)	k
MIT vanes	2	none	0.353	0.855	0.101	22.5	1.02
Logarithmic vanes	2	none	0.482	0.786	0.054	21.2	1.04
MIT vanes	2	internal	0.293	0.889	0.045	19.7	1.52
Logarithmic vanes	3	none	0.304	0.874	0.075	19.0	1.04
MIT vanes	3	internal	0.338	0.865	0.039	16.3	1.52
Logarithmic vanes	3	external	0.117	0.958	0.037	17.1	1.46

Note: CV is the coefficient of variation, γ_{L1} is the uniformity index, I is the turbulence intensity, u_{avg} is the mean velocity, and k is the loss factor

7. Conclusion

A CFD study was conducted to determine a theoretically optimised shape for the logarithmic vanes. The effect of varying curvature distribution was investigated and it was found that a H/W ratio of 0.7 represents a good trade-off. A further study examined the effect of varying the gap-to-chord ratio, and it appears that a ratio of 0.230 was best. These results were applied to 3D print the physical logarithmic vanes.

The flow downstream of the flow contraction is shown to be very steady and uniform, with an index of uniformity of 0.986 and a turbulence intensity of 0.5%. It was deemed a sufficiently controlled experimental environment to test the various turning vane configurations. The screenless MIT produce highly unsteady flow due to strong oscillations in flow velocity. Due to their large expansion ratio and relatively large gap-to-chord ratio, these oscillations might be a sign of diffuser stall. The logarithmic vanes at times also exhibited similar unsteadiness, though to a much lesser extent. Furthermore, the oscillations from the logarithmic vanes could be suppressed through the use of an external wire screen, while the oscillations from the MIT vanes could only be eliminated with an internal screen.

In terms of the pressure loss factor, all screenless vanes had similar performances. The logarithmic vanes with an external screen have a slightly increased pressure drop but also produce the most uniform flow. It appears that the flow exiting MIT vanes with an internal screen is also very uniform. However, due to the overturning of the flow in this configuration, the uniformity does not translate downstream. Therefore, where the use of a coarser screen is required (i.e., in water), the author recommends the use of the logarithmic vanes over the modified version of the MIT-style vanes.

Conceptually, there are additional advantages to employing a single external wire screen downstream of the vane cascade, rather than using internal screens. It is challenging to install

wire screens within a vane channel in a precise manner that will not disturb the flow, especially if the assembly is to be submerged. By comparison, a single external screen is easier to manufacture, access, install, and maintain. Considering this, significant cost savings are to be expected by opting for an external screen, especially considering that a typical ocean basin might need thousands of expansion vanes. Furthermore, the internal screens are arranged diagonally to the flow. Therefore, the wire screen on the outside of the turn is further upstream than the wire screen on the inside of the turn. This allows a larger boundary layer to develop downstream of the outer turn, reducing uniformity in the flow channel.

8. References

- [1] R. W. Fox and S. J. Kline, "Flow regimes in curved subsonic diffusers," *Journal of Basic Engineering*, pp. 303-312, 1962.
- [2] A. Baron von Hohenhau and V. Năsui, "Review of Turning Vanes, Curved Diffusers and their Role in Compact Wind and Water Tunnels," *Acta Technica Napocensis*, vol. 65, no. 3S, 2022.
- [3] H. B. Bijvoet, "Design and characterization of a test facility for large angle diffusers (Thesis)," TU Delft, Delft, 2019.
- [4] D. S. Miller, *Internal Flow Systems*, Cranfield: BHRA (Information Services), 1990.
- [5] S. J. Kline, Director, *Flow Visualization*. [Film]. USA: National Committee for Fluid Mechanics Films, 1963 (<https://www.youtube.com/watch?v=nuQyKGuXJOs>).
- [6] Y. T. Khong, N. Nordin, S. M. Seri, A. N. Mohammed, A. Sapit, I. Taib, K. Abdullah, A. Sadikin and M. A. Razali, "Effect of turning angle on performance of 2-D turning diffuser via Asymptotic Computational Fluid Dynamics," in *IOP Conf. Series: Materials Science and Engineerin1g2*, Songhkla, 2017.
- [7] L. Prandtl, C. Wieselsberger and A. Betz, "Ergebnisse der Aerodynamischen Versuchsanstalt zu Göttingen," R. Oldenbourg, Berlin, 1920.
- [8] A. Sahlin and A. V. Johansson, "Design of guide vanes for minimizing the pressure loss in sharp bends," *Physics of Fluids*, vol. 8, pp. 1934-1940, 1991.
- [9] B. Lindgren, J. Österlund and A. V. Johansson, "Measurement and calculation of guide vane performance in expanding bends for wind-tunnels," *Experiments in Fluids*, vol. 24, pp. 265-272, 1998.
- [10] B. Lindgren and A. V. Johansson, "Design and Evaluation of a Low-Speed Wind-Tunnel with Expanding Corners," Royal Institute of Technology, Stockholm, 2002.
- [11] B. Lindgren and A. V. Johansson, "Evaluation of a new wind tunnel with expanding corners," *Experiments in Fluids*, vol. 36, p. 197-203, 2004.
- [12] M. Drela, A. Huang and D. Darmofal, "Screened expanding turning-vane concept," *Experiments in Fluids*, pp. 61-75, 2020.
- [13] K. Breuer, M. Drela, X. Fan and M. Di Luca, "Design and Performance of an Ultra-Compact Low-Speed Low-Turbulence level Wind Tunnel for Aerodynamic and Animal Flight Experiments," in *AIAA AVIATION 2020 FORUM*, VIRTUAL EVENT, 2020.
- [14] T. P. Chong, P. F. Joseph and P. O. A. L. Davies, "A parametric study of passive flow control for a short, high area ratio 90 deg curved diffuser," *Journal of Fluids Engineering*.
- [15] A. Baron von Hohenhau, "Parameterising the Geometry of Curved Diffusers and Expansion Vanes Using Logarithmic Spirals," *Acta Technica Napocensis*, vol. 65, no. 3S, 2022.
- [16] A. Baron von Hohenhau, "Efficacy of Using the Loss Factor to Estimate the Power Requirements of Wind and Water Tunnels with Varying Cross Sections," vol. 1, pp. 27-35, 2023.
- [17] A. Baron von Hohenhau, "Design and Performance of a Low-Cost Subsonic Wind Tunnel," *Carpathian Journal of Electrical Engineering*, vol. 17, no. 1, pp. 139-156, 2022.
- [18] A. Baron von Hohenhau, "Review and Comparison of Flow Measurement Techniques," *Scientific Bulletin, Fascicle: Mechanics, Tribology, Machine Manufacturing Technology*, ISSN 1224-3264, vol. 2022, no. XXXVI, pp. 27-31, 2022.
- [19] C. Zhang, S. Vasilevskis and B. Kozlowski, "Particle Image Velocimetry User Guide," Aalborg Universitet, Aalborg, 2018.

COPY OF THE TABLE OF CONTENTS OF THE DOCTORAL THESIS

ABBREVIATIONS.....	3
1. Introduction.....	5
1.1. Abstract.....	5
1.2. Thesis Content.....	5
1.3. Objectives and Purpose of the Current Research.....	6
1.4. The Scientific novelty of the research.....	8
CURRENT STATE OF KNOWLEDGE	9
2. Current Theoretical Research.....	10
2.1. Boundary Layer Theory.....	10
2.2. Law of the Wall	11
2.3. Loss Factor Overview.....	13
2.4. Loss factor in diffusers.....	14
2.5. Secondary flows.....	17
2.6. Evolution of technical achievements.....	20
2.7. Turning vanes – existing achievements	21
2.8. Types of turning vanes	27
2.9. Straight diffusers – existing achievements	31
2.10. Curved diffusers – existing achievements.....	34
2.11. The flow regime in curved diffusers	36
2.12. Comparing straight and curved diffusers.....	40
2.13. Expansion vanes - combining vanes and diffusers.....	41
2.14. Lindgren expansion vanes and experiments	42
2.15. Drela expansion vanes and experiments.....	44
2.16. Summary of the Current State of Knowledge	45
3. Experimental Measurement Techniques	47
3.1. Measuring pressure	47
3.2. Multi-hole probes.....	49
3.3. Particle image velocimetry	51
3.4. Laser Doppler Velocimetry.....	53
3.5. Choice of Tracer Particle.....	54
3.6. Comparison of measurement techniques.....	56
3.7. Conclusion and Choice of Measurement Technique.....	59

PERSONAL CONTRIBUTIONS	60
4. Development of a Novel Turning Vane Shape.....	61
4.1. A brief overview of logarithmic spirals	62
4.2. Construction of 90° logarithmic diffusers	64
4.3. Constructing non-90° diffusers.....	77
4.4. Comparing diffuser types and geometries.....	81
4.5. Logarithmic diffuser length and expansion angle	83
4.6. Constructing vanes from logarithmic spirals.....	84
4.7. Summary of logarithmic vane construction	85
5. A testing environment for turning vanes.....	86
5.1. Wind Tunnel Design and Construction	86
5.2. Wind Tunnel Power Requirements.....	104
5.3. Test Section Design and Construction	107
5.4. Traverse System Construction	115
5.5. Pressure Measurement System	119
5.6. Custom Python Scripts.....	123
5.7. Summary of the Experimental Setup and Processing	129
6. Conducting Flow Experiments.....	130
6.1. Quantifying flow uniformity and turbulence	131
6.2. CFD analysis	137
6.3. Characterising the Wind Tunnel	155
6.4. Testing the expansion vanes.....	176
6.5. Summary Comparison of Performance	185
6.6. Summary of Experimental Results	189
7. General Discussion.....	190
8. Final Conclusions.....	192
8.1. General Conclusions	192
8.2. Thesis originality and innovative contributions	193
8.3. New Elements within the Thesis.....	194
8.4. Capitalising on Theoretical and Experimental Research.....	195
8.5. Future Research Directions.....	195
9. References	196
10. Indices	202
10.1. Index of Figures	202
10.2. Index of Tables	209
11. Appendices	210
11.1. Appendix A - Project budget and financing	210
11.2. Appendix B - Code to generate logarithmic spirals.....	212
11.3. Appendix C - Vanes at the University of Oxford.....	219
11.4. Appendix D - Vanes at Khalifa University	221
12. List of Publications.....	224